Fuel 230 (2018) 376–389

Contents lists available at ScienceDirect

Fuel

journal homepage: www.elsevier.com/locate/fuel

Full Length Article

Investigation of the reduction kinetics of high loaded CuO-based materials suitable for the Ca/Cu looping process

L. Díez-Martín*, I. Martínez, G. Grasa, R. Murillo

Instituto de Carboquímica, ICB-CSIC, M Luesma Castan 4, 50018 Zaragoza, Spain

ARTICLE INFO

Keywords:
Ca/Cu looping process
CuO-based materials
Reduction kinetics
Shrinking core model

ABSTRACT

In this work, the reduction reactions of highly loaded CuO-based materials with H_2, CO and CH_4, have been investigated. The oxygen transport capacity of the materials was barely affected (i.e. losses around 5%) along 100 reduction/oxidation cycles at 1123 K tested in TGA. The experimental results suggested that a shrinking core model (SCM) with chemical reaction control is able to predict the reduction conversion of highly loaded CuO-based materials in powder and pellet form, and the kinetic parameters were accordingly determined to this model. The activation energy values obtained for the materials supported over Al_2O_3 and $MgAl_2O_4$ are in the range of 10 kJ mol^{-1} for H_2, 25 kJ mol^{-1} for CO and 60 kJ mol^{-1} for CH_4, in agreement with results published in the literature, indicating that using Al_2O_3 or $MgAl_2O_4$ as support has not a significant effect on the reactivity. It has been found that internal diffusion plays a role for the highly loaded CuO-based in pellet form when supported over MgAl2O4 and when using CO and CH_4 as reducing agents. Mixtures of reducing gases have been also tested in the TGA for a pellet using Al_2O_3 as support and the experimental results have been successfully fitted using the kinetic parameters previously determined. Finally, a simplified energy balance for the reactions involved in the reduction/calcination stage of the Ca/Cu process has been performed to determine operational conditions in which the reaction fronts for both reactions proceed together in the reactor. The results indicate that the materials tested present suitable reaction kinetics to sustain the reduction/calcination stage.

1. Introduction

Hydrogen consumption worldwide is mainly driven by the oil refining and chemical's production sectors, whereas its use as energy carrier to be converted into electricity, mechanical energy and/or heat is still beginning to emerge [1]. Despite the share of the hydrogen production from steam reformers barely represents a 3% in the global share of CO_2 emissions [2], the hydrogen demand will grow in the coming decades boosted by an increasingly ammonia production for the fertilizers' industry driven by the demographic growth of developing countries like China, as well as by the increase in the use of hydrogen for hydrotreating and hydrocraking processes in the refining industry. Moreover, the even more restricting policies regarding the decarbonisation of the power production sector will boost the demand of hydrogen to be used as fuel in boilers and process heaters [3,4], as well as fuel in the transport sector [1]. On the other hand, it has been recognised the reduction of CO_2 emissions from large stationary sources as one of the solutions needed for contributing to achieve the near term goals for climate stabilization [5]. In this way, large scale hydrogen production combined with CO_2 capture and permanent storage is presented as one of the potential routes to decarbonize the energy and/or industrial sectors.

Steam methane reforming (SMR) constitutes the dominant technology for hydrogen production at commercial scale, being responsible for half of the hydrogen production worldwide. However, this technology has important drawbacks related to the stringent conditions of high pressure and high temperature needed in the fired tubular reformer of this process [6]. Therefore, different options for hydrogen production have been proposed in the literature with the aim of improving the efficiency of the process as well as of reducing the production costs with respect to this well-established technology. In the last years, different processes for H_2 production that combine reforming reaction with CO_2 separation in a single step have gained importance because of the higher yields of H_2 achieved by these systems [7–11].

In this context, the sorption enhanced reforming (SER) of methane has been widely studied as a process where hydrogen production through steam reforming and water gas shift (WGS) reactions occur in the presence of a CO_2 sorbent (usually CaO) that reacts in situ with the CO_2 as soon as it is formed (Eq. (1)) [12–15]. The combination of the chemical and separation reactions in a single reactor simplifies the

* Corresponding author.
E-mail address: ldiezmartin@icb.csic.es (L. Díez-Martín).

https://doi.org/10.1016/j.fuel.2018.05.054
Received 30 November 2017; Received in revised form 9 March 2018; Accepted 10 May 2018
Available online 25 May 2018
0016-2361/

Nomenclature

T	temperature (K)
P	pressure (bar)
X_{red}	reduction conversion (−)
m_{ox}	mass of the fully oxidized material (mg)
m_{red}	mass of the fully reduced material (mg)
m(t)	mass of the material at a specific time (mg)
OTC	oxygen transport capacity (mg O/mg oxidized material)
t	time (s)
L	particle or pellet radius (m)
b_i	stoichiometric coefficient of the CuO reduction reaction for the gas i (−)
k_{si}	reaction rate constant for gas i ($mol^{1-n} m^{3n-2} s^{-1}$)
C_{gi}	gas concentration for species i ($mol\,m^{-3}$)
n	reaction order
ko	pre-exponential factor ($mol^{1-n} m^{3n-2} s^{-1}$)
R	universal gas constant (J/mol K)
Ea	activation energy (J/mol)
r_c	radius of unreacted core or reaction front (m)
h_m	gas film mass transfer coefficient (m/s)
D_e	effective mass diffusivity (m^2/s)
D_{pore}	mass diffusivity inside mesopores (m^2/s)
D_i	mass diffusivity of species i (m^2/s)
D_{Kn}	Knudsen diffusivity (m^2/s)
d_{pore}	pore diameter (m)
M_i	molecular weight of the specie i (g/mol)
ΔH	reaction enthalpy (kJ/mol)

Acronyms

SMR	steam methane reforming
SER	sorption enhanced reforming
WGS	water gas shift
TGA	thermogravimetric analyzer
S/C	steam to carbon molar ratio
SCM	shrinking core model
CGSM	changing grain size model

Greek letters

τ_i	time required for complete conversion (s)
ρ	density of the material (kg/m^3)
ρ_b	molar density of the CuO in the particle ($mol\,m^{-3}$)
τ_{pore}	tortuosity of the pores (−)
ε	porosity (−)
υ_i	diffusion volume for component i (m^3/mol)

process and improves the efficiency since the conversion towards hydrogen production is greatly improved. Hydrogen concentrations of around 95 vol.% (dry basis) can be reached in one step at temperatures of 923–1023 K [12,15], without the need of a subsequent WGS stage for improving CO conversion. Moreover, global reaction of this SER process is slightly exothermic and no additional energy would be required within the hydrogen production step. However, to be able to operate in continuous mode, the sorbent containing the $CaCO_3$ formed during the SER process needs to be regenerated by calcination (Eq. (2)), which requires from a large amount of energy due to the endothermicity of the reaction.

$$CH_4(g) + CaO(s) + 2H_2O \rightleftarrows CaCO_3(s) + 4H_2(g) \quad \Delta H_{298\,K} = -13.7\ kJ/mol \tag{1}$$

$$CaCO_3(s) \rightarrow CaO(s) + CO_2(g)) \quad \Delta H_{298\,K} = +178.5\ kJ/mol \tag{2}$$

Among the different alternatives proposed in the literature for providing the energy needed during the calcination in this process, this work focuses on a novel scheme for the SER process based on coupling a Cu/CuO chemical loop for supplying the energy needed for $CaCO_3$ calcination [7,16]. This process follows the basic scheme shown Fig. 1, which was originally proposed to be carried out in a series of fixed-bed reactors operating in parallel where temperature and pressure are accommodated to make each reactor pass through every stage of the process. In the first stage, an enriched stream of H_2 is produced through a SER process when feeding natural gas/methane and steam to the reactor in the presence of a reforming catalyst, a CaO-based sorbent and a Cu-based solid. Preliminary studies about this process have indicated that the proper conditions for operating this process stage correspond to 873–1023 K, steam-to-methane molar ratios (S/C) between 2.5 and 5, and pressures between 10 and 35 bar [9,17]. In the second step, the Cu-based material is oxidized with diluted air at a high pressure. The maximum temperature reached during this stage needs to be controlled through the oxygen content and the temperature of the feed to avoid the prompt decomposition of the $CaCO_3$ and the problems related to the agglomeration of the Cu [18]. The final and next stage of the process consists of the calcination of the $CaCO_3$ formed during the SER stage by means of the energy provided by the simultaneous reduction of the CuO present in the solid bed with a fuel gas containing CH_4, H_2 and/or CO.

$$CuO(s) + H_2(g) \rightarrow Cu(s) + H_2O(g) \quad \Delta H_{298\,K} = -86.9\ kJ/mol\ CuO \tag{3}$$

$$4CuO(s) + CH_4(g) \rightarrow 4Cu(s) + 2H_2O(g) + CO2(g) \quad \Delta H_{298\,K} = -181.45\ kJ/mol\ CuO \tag{4}$$

$$CuO(s) + CO(g) \rightarrow Cu(s) + CO_2(g) \quad \Delta H_{298K} = -127.8\ kJ/mol\ CuO \tag{5}$$

This stage is operated at atmospheric pressure for keeping the calcination temperature under reasonable limits (i.e. 1123–1143 K) for this process. A suitable $CuO/CaCO_3$ molar ratio in the solid bed is needed in order to ensure that total calcination of the $CaCO_3$ formed is achieved using the heat released during CuO reduction without any external energy supply [19]. Composition of the fuel gas used in this stage influences the proportion of Cu/Ca needed in the process, being the highest Cu/Ca ratio of 3.1 needed if pure CH_4 is used and the lowest value of 1.3 if pure CO is employed as reducing gas [9].

Significant progress has been made concerning material's development, reactor modeling and process design in the last years for this Ca/

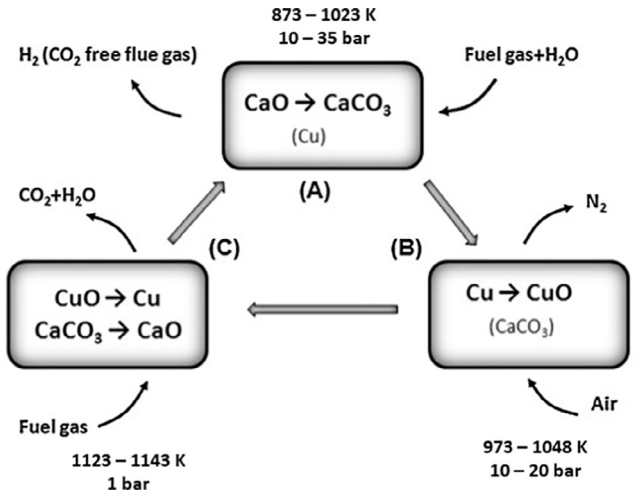

Fig. 1. Conceptual scheme of the Ca/Cu looping process.

Cu process, as recently reviewed in [20]. The reduction/calcination stage that constitutes the core of this process has been successfully validated at industrially relevant conditions for this technology [21]. The inherent advantages of this concept make it suitable to be integrated as part of hydrogen and/or a power production process. Mass and energy balances of a standalone hydrogen production plant [22] and a natural gas combined cycle power plant [23] have been published in the literature, demonstrating its potential with respect to state of the art technologies. Dynamic behavior of the different reaction stages shown in Fig. 1 has been also carefully studied [24,25], considering that the initial conditions of each step corresponds to the final conditions of the previous one. Such dynamic models have been useful for designing optimized process schemes for the Ca/Cu process that aim at maximizing the CO_2 capture efficiency and/or minimizing the number of parallel reactors [24,26].

The Ca/Cu looping process requires three functional materials, which must be able to be carbonated and calcined maintaining high CO_2 uptake (in the case of CaO-based sorbents), to be oxidized and reduced showing high O_2 carrying capacity (in the case of Cu-based solids) or to exhibit sufficient catalytic activity (in the case of the reforming catalyst) over many cycles. In recent years, substantial progress has been made in the development of high-performance materials with direct application to the Ca/Cu looping process, as their characteristics are not very far from those of functional materials required in processes as chemical looping combustion (CLC) and conventional SER processes [7,9] . As already reported in the literature, the presence of inert species in the solid bed material impacts negatively the energy balance of the process since they behave as a thermal ballast within the reactor, and so consume part of the energy released in the reactor for heating up. In this way, a great research effort is being done in the synthesis and testing of functional materials for the Ca/Cu process with the aim of minimizing the amount of inert and so increase the amount of active phase.

A key aspect for the development of the Ca-Cu H_2 production process is to have materials with optimum properties for cyclic operation. The ratio Cu/Ca in the process will be determined by the requirements in the calcination step [7], and in order to reduce the thermal ballast of the inert fractions comprising the materials, it is necessary to maximize the active phase content of both the CuO-based and CaO-based materials [7,9]. Focused on the Cu-based material, according to the preliminary balances solved by Fernández et al. for the Ca/Cu process, materials with CuO loads between 60 wt% and 80 wt% would be preferred in this process [9,24]. In this way, several authors have developed materials with copper contents over 60%wt (metal load) onto Al_2O_3 by different synthesis procedures as freeze granulation and mechanical mixing [27]; or impregnation methods [28]. There are also materials with contents up to 80% wt. (metal oxide) on to different supports (sepiolite, SiO_2, TiO_2, ZrO_2) prepared again by mechanical mixing [27]. On the other hand, the CuO materials with the greatest Cu loads (70–87 wt% of CuO) have been synthesized by Imtiaz et al. by co-precipitation onto Al_2O_3 [29] obtaining promising results with regard to the chemical stability along 25 redox cycles. Despite of these results, it is still needed to demonstrate the chemical and mechanical stability of high Cu load materials after sufficient number of reduction/oxidation cycles, in powder and pellet form, according to the cyclical operation of the Ca/Cu looping process.

There are numerous works in the literature on the determination of reduction kinetics of CuO materials containing a wide range of Cu loads on to different supports [28,30–44], mainly for application in CLC processes. Different gas–solid models such as the shrinking core model (SCM) [28,30,32,36,37,39], the changing grains size model (CGSM) [31,39] and nucleation models [33,45] have been reported to determine the kinetic parameters of reduction reactions of different metal oxide materials. The SCM model has been successfully applied to determine the kinetic parameters for the reduction reaction of different metal oxides [28,32,36,39]. Ishida et al. [36] first tested the SCM on NiO-based particles and considered the contribution of external mass transfer, internal mass transfer and chemical reaction on the evolution of materials conversion. They found that the reduction rate was mainly controlled by the chemical reaction that it was strongly influenced by temperature. Later on, García-Labiano et al. [32] applied the SCM to determine the kinetic behavior of a 10%wt CuO/Al_2O_3 powdered material prepared by impregnation. These authors found that the reduction reaction by H_2 was controlled by the diffusion of the reacting gas through the product layer at low temperatures (below 723 K) and by the chemical reaction at high temperatures (starting from 1073 K). A low dependence of the reaction rate with temperature was observed with the activation energy values varying from 14 to 60 kJ mol^{-1} depending on the reducing gas used. Concerning the use of highly loaded Cu materials in pellet form, García-Lario et al. [28] successfully applied the SCM with chemical reaction control for the reduction reaction of a CuO-based pellet with 60%wt of CuO over Al_2O_3 prepared by impregnation. The activation energies found (i.e. from 23 to 74 kJ mol^{-1}) match fairly well the values reported in the literature, with reaction orders between 0.9 and 1. Most of the works published on the literature on the reduction kinetics for Cu-based materials focused on the kinetics in particle/powder form, whereas the use of fixed bed reactors in the Ca/Cu looping process makes it necessary to work with the materials in pellet form. Finally, it is also important to remark that the effect of total pressure on the reduction reactions of CuO-based oxygen carriers has been studied in a recent work by San Pio et al. [43] and no influence of this parameter was found. The present work is focused on determining the reduction reaction kinetics with H_2, CO and CH_4 of two high load CuO-based materials in powder and pellet form, which are suitable for the Ca/Cu looping process. The effect of the nature of the inert support on the materials reactivity have been assessed, as well as the effect of the reaction temperature, the reducing agent used and the partial pressure of the reducing gas. Moreover, the evolution of the materials conversion with time under expected conditions of the reduction/calcination stage of the Ca/Cu process has been assessed experimentally and compared with the predictions of the proposed reaction model. Finally, the coupling between the heat released by one pellet of CuO-based material and the heat demand for the calcination of the corresponding amount of $CaCO_3$ is assessed, aiming to compare the matching of the reduction and calcination reaction fronts within the reduction/calcination stage of the studied process.

2. Experimental section

2.1. Materials

Two different materials synthesized by co-precipitation with Cu contents around 65%wt have been tested in this work [46]. The first Cu-based material contains Al_2O_3 as support and has been synthesized by Johnson Matthey PLC (referred as Cu65Al_COP), whereas the second one is supported on $MgAl_2O_4$ and prepared by ICB-CSIC (Cu65MgAl_COP). These materials were selected between a wide range of CuO-based materials prepared by different synthesis routes and onto different supports with Cu contents between 48.1 and 75.0%wt [46]. The procedure of the synthesis route of the materials consists of preparing separate nitrate solutions of Cu, Al or Mg and mixing them adjusting before the pH adding Na_2CO_3.The resulting solution was stirred and filtered. The precipitate formed was washed several times with distilled water to remove excess nitrate and alkali ions. Then, the resulting solid was dried overnight at 393 K in an oven and finally calcined in a muffle furnace. In the case of the material supported onto $MgAl_2O_4$ synthesized at ICB-CSIC, the nitrate solutions were mixed and the pH of the resulting mixture was adjusted at 9.8 adding Na_2CO_3. The calcination for this material was carried out at 1243 K during 2 h keeping a heating rate of 50 °C/min. Part of the material was kept in powder form and part was used for producing pellets. In the last case, Johnson Matthey PLC incorporated small quantities of a binder to the pellets which

makes the Cu content in the pellet slightly reduce with respect to that in the powder. Concerning the pellets using $MgAl_2O_4$ as support, they were prepared without using any additional binder, and so the composition of the powder and that of the pellet match. Therefore both materials are presented in principle as suitable candidates for the process, therefore it is needed to know the redox kinetics of both materials in order to select the more suitable material for the process.

Both CuO-based materials have been widely characterized through different techniques. The elementary composition of fresh materials was determined by ICP-OES using a spectrometer (SPECTROBLUE OF AMETEK), the presence of crystalline species in fresh and cycled samples was identified by X-ray Diffractometry Analysis (XRD) using a X-ray diffraction equipment of polycrystalline powder Bruker D8 Advance. In this way, the X-ray diffraction equipment has been worked with Bragg-Brentano theta-theta geometry and using a Bruker's EVA software to carry out the phase assignment and the crystal size has been determined using the Pawley method and the calculations were made applying the software DIFFRACplus TOPAS considering a k Serrer constant of 0.89 [47]. Temperature programmed reduction (TPR) analysis was used to study the temperatures of reducible species present in each material. These tests are carried out in the Micromeritics AutoChem II equipment, subjecting the sample to a temperature program in a flow of 10% H_2 in Ar and monitoring the variation of the H_2 concentration in the gas by means of a thermal conductivity detector. The determination of the specific surface area is carried out by physisorption of nitrogen at 77 K in the equipment ASAP 2020 of Micromeritics, applying the BET method to the obtained isotherm. The solid density The determination of the solid density has been carried out by helium pycnometry in the ACCUPYC II equipment of Micromeritics by measuring the amount of helium displaced by the sample. Finally, the porosimetry of the samples were determined in the AUTOPORE V equipment of Micromeritics. In addition, cross section SEM images of the pellets at different conversion levels were taken using a SEM-EDX Hitachi S-3400N microscope with variable pressure up to 270 Pa with Röntec XFlash Si (Li) EDX analyzer. Table 1 compiles the main physical and chemical properties obtained from these characterisation techniques for both CuO-based materials in powder and pellet form.

2.2. Experimental procedure

A thermogravimetric analyzer (TGA-CI Electronics Ltd.) has been used in this work to analyze the stability of the materials as well as the reduction reactions kinetics with H_2, CO and CH_4. This equipment consists of two concentrically quartz tubes located inside a furnace (see Fig. 2). The solid sample was introduced in a platinum basket placed at the bottom of this device. The gas mixture is regulated through mass flow controllers and it is fed laterally from the upper part of the quartz tube, flows down to pass around the same and exits the tube through a concentric tube located in the inner part as indicated in Fig. 2. The thermocouple that measures the temperature of the sample is located at the bottom of the apparatus close to the basket. A continuous flow of N_2 is feed through the head of the TGA as a protection measure. During the experimental campaign, the system was programmed to collect data every second of reaction. Since a gas flow is introduced into the reactor less than 5 s are required until the flow reach the sample. Once in contact with the sample, the gas reacts and leaves the reactor through the upper part of the thermobalance. The system was programmed to collect data every second of reaction, and the real time sampling is about 1.6 s.

2.2.1. Chemical stability

The chemical stability of the materials has been tested in the TGA under isothermal conditions through 100 reduction/oxidation cycles at 1123 K. These tests were carried out using 15 mg of sample in powder form or one individual pellet in the TGA apparatus. A constant total flow of 280 ml/min of gas was used for the experiments. These stability tests consisted of a reduction period using a gas stream with 20 vol.% H_2 in N_2, and an oxidation stage in 20 vol.% O_2 in N_2. An intermediate purge period of 1 min in pure N_2 was introduced between each reduction/oxidation stage. Heating and cooling of the sample at the beginning and at the end, respectively, of the stability tests were carried out in pure N_2. The change in the weight of the material after oxidation was used to determine the Cu load in each material. The conversion of the CuO-based materials during the reduction reaction with H_2 has been calculated through the mass change measured in the TGA under specific conditions. Reduction conversion is defined by Eq. (6) where m(t) represents the mass sample at each time and m_{ox} is the mass of the fully oxidized material (i.e. with the Cu in the form of CuO).

$$X_{red} = \frac{m_{ox} - m(t)}{m_{ox} \cdot OTC} \quad (6)$$

OTC represents the oxygen transport capacity of the material along multiple reduction/oxidation cycles, which is defined by the following formula:

$$OTC = \frac{(m_{ox} - m_{red})}{m_{ox}} \quad (7)$$

In this expression, m_{red} corresponds to the mass of the completely reduced CuO-based material.

2.2.2. Determination of the kinetic parameters

The reduction reaction kinetics for the CuO-based materials have been determined in the TGA for the three different reducing gases used in the Ca/Cu process (i.e. H_2, CO and CH_4). Preliminary tests were performed to assess the amount of sample required for the total flow of 280 ml/min used previously to avoid any mass transfer limitation due to sample amount and sample pan geometry, as well to any gas film resistance. A mass of 10 mg was finally selected for the kinetic tests for the materials in the powder form, whereas one individual pellet was loaded when studying the pelletized form.

The effect of temperature (from 973 to 1143 K) and reacting gas concentration were assessed for the reduction reaction for determining the kinetic parameters for both materials in powder (from 5 to 20%vol.) and pellet (from 10 to 40%vol.) forms. To determine the reaction order, consecutive oxidation/reduction cycles were performed at a constant temperature of 1123 K varying the reducing gas partial pressure. On the other hand, to determine the pre-exponential factor and activation energy of the kinetic constant, tests were made through consecutive

Table 1
Main physical properties of the co-precipitated materials tested in this work.

POWDERED MATERIALS	Cu65Al_COP	Cu65MgAl_COP
Support material	Al_2O_3	$MgAl_2O_4$
wt% Cu	$65.5 \pm 6.23 \times 10^{-2}$	$65.0 \pm 5.17 \times 10^{-2}$
%OTC (mgO/mg material)	$0.164 \pm 2.41 \times 10^{-4}$	$0.163 \pm 1.57 \times 10^{-4}$
Particle diameter (μm)	75	60.5
ε (oxidized particles)	60	75
ρ (kg/m^3)	5440	5510
ρ_b (molCuO/m^3)	55,407	56,100
BET surface area (m^2/g)	21	19
CuO crystal size (nm) – Fresh sample	66.1	86.6
CuO crystal size (nm) – Cycled sample	61.3	63.1
PELLETS	P_Cu65Al_COP	P_Cu65MgAl_COP
wt% Cu	$60.1 \pm 5.53 \times 10^{-2}$	$64.8 \pm 4.89 \times 10^{-2}$
%OTC (mgO/mg material)	$0.149 \pm 1.35 \times 10^{-4}$	$0.163 \pm 1.22 \times 10^{-4}$
Pellet diameter (m)	3.3×10^{-3}	3×10^{-3}
Pellet height (m)	3.3×10^{-3}	3×10^{-3}
weight oxidized (kg)	65.6×10^{-6}	48.0×10^{-6}
ρ (kg/m3)	2240	2250
ρ_b (molCuO/m^3)	21,186	22,910
d_{pore} (nm)	22	50
ε (oxidized pellet)	48	43
BET surface area (m^2/g)	24	20

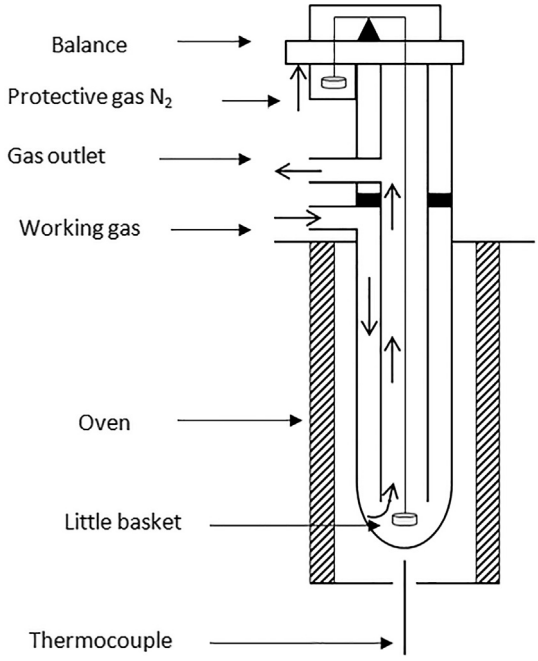

Fig. 2. Thermogravimetric apparatus used during the reduction tests.

oxidation/reduction cycles varying the temperature during the reduction period with a constant reducing gas concentration of 10%vol. of reducing gas in N_2. In all these tests, oxidation stage was carried out at the same temperature that the previous reduction and with a gas composition equal to 20%vol. O_2 in N_2. An intermediate 1 min period of purge in N_2 was introduced between each oxidation and reduction period for cleaning the quartz tube for any reacting specie for the next stage. For experiments made with CO and CH_4, a similar flow of CO_2 was also introduced in the reaction atmosphere to avoid any carbon deposition on the solid.

2.2.3. Reduction tests with process gas composition

Regarding the reduction/calcination stage of the Ca/Cu process, different configurations have been proposed in the literature when studying this process at large scale [20], which will determine the composition of the reducing gas used. Initial configurations of the Ca/Cu process proposed the use of an intermediate step between the reduction/calcination step and the SER one to adequate bed temperature for the SER through the reforming of additional methane with a low S/C ratio. In such configuration, the syngas produced in this cooling step is used as feed gas in the reduction/calcination stage. Due to the high temperature of the solid bed at the beginning of the cooling, this syngas will be rich in H_2 with considerable amounts of CO since the carbonation reaction (and so WGS) is not favored at such temperatures [9,24]. On the other hand, alternative configurations where the reduction/calcination stage is fed with a rich-CH_4 gas coming from an adiabatic pre-reforming stage have been also considered [22]. Such configuration will allow reducing the total number of reactors operating in the Ca/Cu process as well as eliminating the higher hydrocarbons present in the natural gas, which may deactivate the catalyst if carbon formation occurs within the solid bed. When using this pre-reforming reactor upwards the reduction/calcination stage, the feed gas to this stage will contain larger amount of CH_4 (i.e. since the pre-reforming stages operates at a lower temperature) than in the previous process configuration. This CH_4 contributes also to the presence of reforming reactions within the solid bed during this reaction stage of the Ca/Cu process, favoring also the cooling down of the solid bed.

Dedicated TGA experiments have been performed using a mixture of H_2, CO and CH_4 during the reduction to reproduce the aforementioned process configurations for the calcination/reduction stage of the Ca/Cu

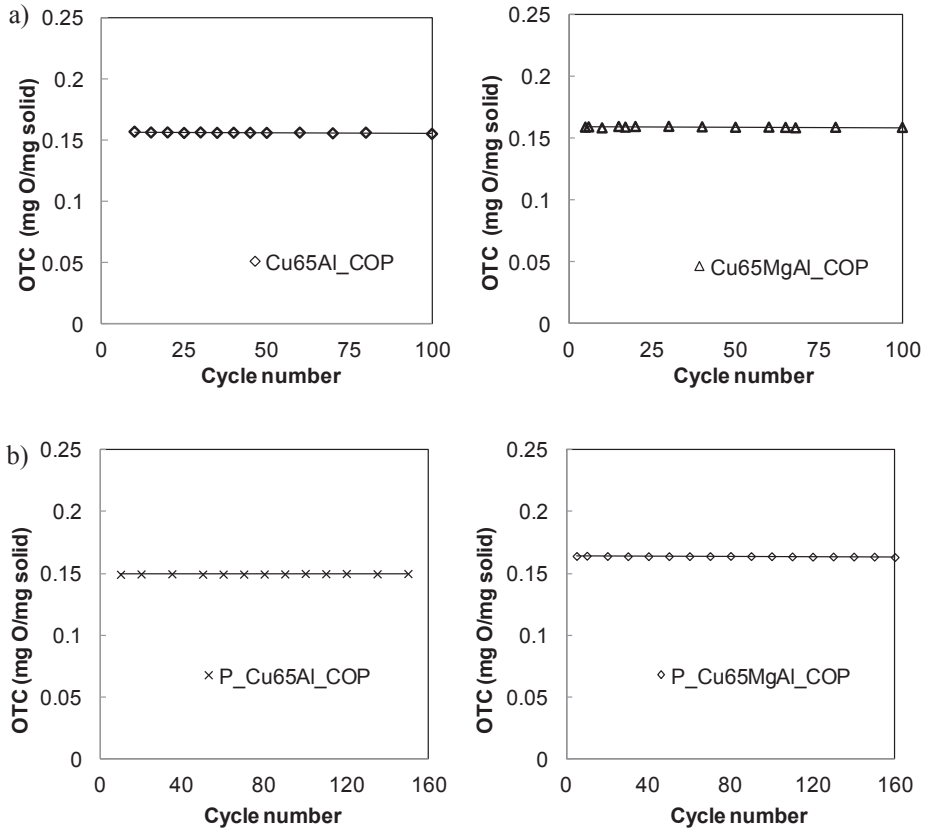

Fig. 3. Evaluation of the oxygen transport capacities for materials supported on to Al_2O_3 and $MgAl_2O_4$, respectively: a) materials in powder form, b) pellets.

process. The objective of these experiments is demonstrating that the kinetic model determined predicts correctly the conversion curves of the CuO-based material pellets under these real process conditions. Concerning the conditions of an intermediate cooling stage between the reduction/calcination stage and the SER one, a syngas composition of 67.5%vol. H_2, 22.5%vol. CO and 10%vol. CO_2 at 1143 K was used [24]. Contrarily, for the conditions where an adiabatic pre-reformer is placed upwards the reduction/calcination stage a syngas containing 45%vol. CH_4, 7.3%vol. H_2, 37.7%vol. N_2 and 10%vol. CO_2 was used [22]. In both cases a total gas flow of 280 ml/min was used. Such compositions have been slightly tuned with respect to those found in the literature to keep a minimum concentration of CO_2 equal to 10%vol. to avoid carbon deposition on the solid. One individual pellet was loaded in the TGA to analyze each stage individually.

Finally, the evolution of the pellet conversion with time under these conditions was used to study the heat releasing rate within the pellet particle with respect to the heat demand rate of a sorbent with a $CaCO_3$ content given by the typical Ca/Cu ratio of 2 proposed in the literature [24]. The kinetic parameters for the calcination of the $CaCO_3$ present in the sorbent have been taken from the literature [48]. This simplified study of the evolution of both reactions with time helped to illustrate the proximity of both reaction fronts in the reactor as function of material's reactivity and temperature.

3. Results and discussion

Fig. 3a shows the OTC of the two CuO-based materials in powder form along the 100 oxidation/reduction cycles performed to check the chemical stability. As appreciated, the OTC of both materials has remained completely stable along the cycles, with variations lower than 5% with respect to the OTC measured for the first cycle. The OTC measured for both materials in powder form is practically the same (i.e. 0.158–0.159 mgO/mg material) as appreciated from Fig. 3. Chemical stability was also measured for the materials in the pellet form under the same conditions as for the powder, and the same good stability along cycles was observed (see Fig. 3b). However, a lower OTC value for the pellet than for the powder form was observed for the Cu65Al_COP material (i.e. 0.149 mgO/mg material), as indicated in Table 1. This reduction is explained by the reduction in the copper content of the solid when pelletizing due to the addition of a binder compound to improve the mechanical resistance of the pellets.

As it can be observed in Table 1 the size of CuO crystals of the fresh and cycled samples has been determined by XRD-analysis for the materials in powder form. In the case of the materials supported over Al_2O_3 the CuO crystals have shown similar sizes in both cases but a significant decrease in size of the CuO crystals in cycled samples has been observed in the materials supported onto $MgAl_2O_4$.

3.1. Kinetic parameters

As anticipated, the kinetic parameters for both CuO-based materials containing approximately 65%wt of Cu have been determined for both powder and pellet forms, using H_2, CO and CH_4 as reducing agents. Concretely, the kinetic parameters for the reduction reaction with H_2, CO and CH_4 were first determined for the materials in powder form, and then the calculated kinetic parameters were used to predict the reduction reactions of the corresponding pellet.

Fig. 4 shows the effect that the reaction temperature (in the range of 973 K–1143 K) has on the reduction conversion of the powdered materials using 10%vol. of each specific reducing gas in N_2. As noticed, the reduction reaction rate was fast in the range of temperatures studied and complete conversion was reached for the three reducing gases tested. A significant effect of the temperature is observed depending on the reducing gas used. The reduction rate with H_2 presented a low dependence with temperature whereas the reduction rate with CH_4 and CO showed a greater variation when temperature changes, which

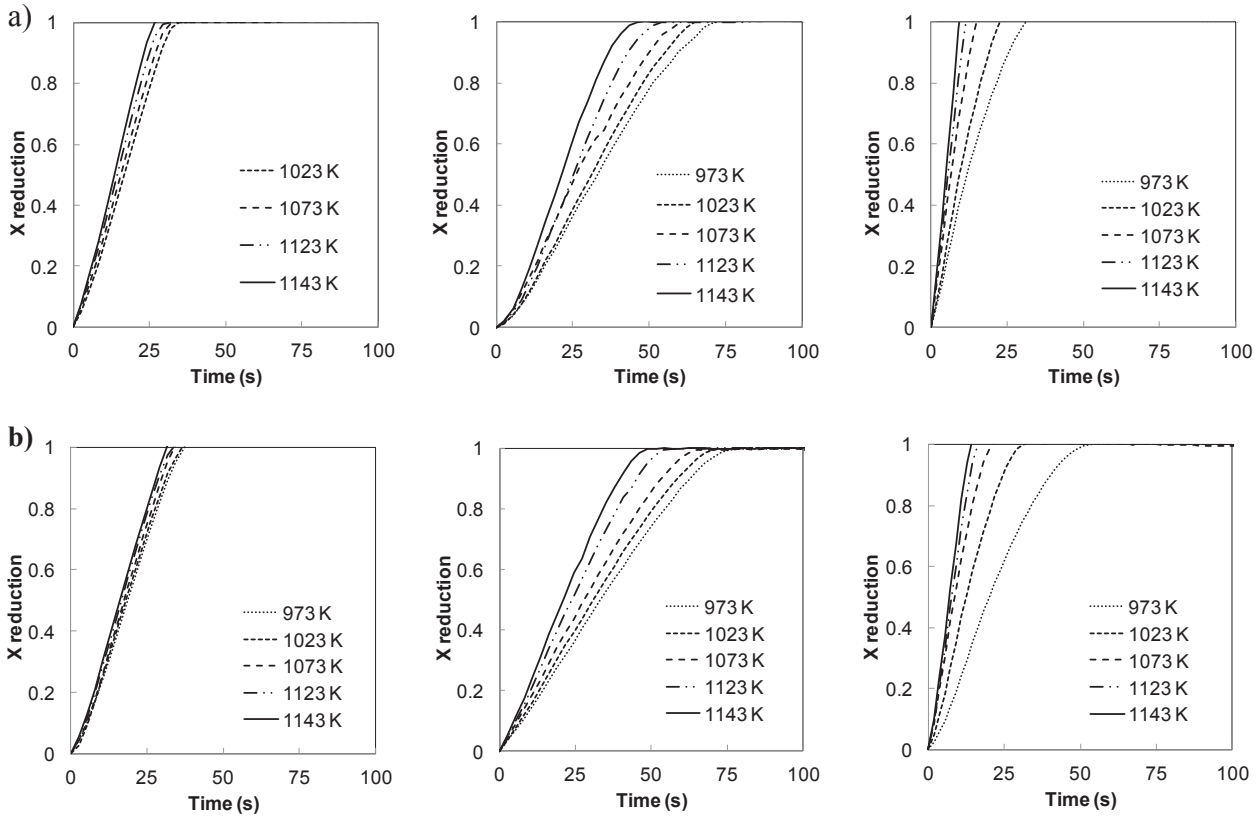

Fig. 4. Effect of temperature on reduction conversion curves of CuO-based particles in powder form.

points out at a higher activation energy values for these gases than for H_2. On the other hand, the straight slope of the reduction curves with H_2, CO and CH_4 represented in Fig. 5 suggests that the reduction kinetics are controlled mainly by chemical reaction [27].

No significant differences can be observed between the reduction conversion curves obtained for both materials at the different temperatures, except for the conversion curves obtained for the lowest temperature of 973 K with CH_4 and CO that show a slower reaction rate for the Cu65MgAl_COP material. The less pronounced final part of the reduction curves with CO and CH_4 at the lowest temperature could indicate that gas diffusion resistance within the particle becomes a controlling factor in the kinetics. An important aspect to highlight is that the materials have shown that for the optimum operating temperature range for the reduction/calcination stage of the Ca/Cu process (i.e. between 973 and 1143 K), the materials reacted faster with H_2 than with the other gases. Although in view of the reduction conversion curves for all gases tested it seems that the reduction reaction with CO was the slowest of the three reduction reactions, it has to be taken into account that according to the stoichiometry (see Eq. (4)) the CH_4 reacts with 4 mol of CuO, and therefore it is not possible to compare the curves of this gas with the conversion curves of the other reducing agents. However, the reaction rate constant during the different reactions of CuO for each reducing agent has allowed to determine that the CH4 is the less reactive gas (see Table 2 for kinetic parameters) in agreement with previous results published in the literature [28,41].

Based on the curves shown in Fig. 4, a shrinking core model (SCM) has been chosen to fit the experimental data for the materials in powder form, based on the experience with other metal compounds under reduction conditions published in the literature [27,28,37,41]. Chemical reaction control and plate-like geometry have been considered to describe the evolution of the conversion profiles of the particles with time [49]. The equation that governs the evolution of the conversion for this model is:

$$\frac{t}{\tau_i} = X_{red} \tag{8}$$

where X_{red} is the conversion, t the time and τ_i represents the time required to achieve complete conversion of the material when using the reducing gas i. This time depends on the reacting gas (i = H_2, CO, CH_4), and it can be determined as:

$$\tau_i = \frac{\rho_b L}{b_i k_{si} C_{gi}^n} \tag{9}$$

where L represents the particle or pellet radius (in m), ρ_b represents the molar density of CuO in the particle (in mol m^{-3}), b represents the stoichiometric coefficient of the CuO reduction reaction depending on the reacting gas evaluated, C_{gi} represents the reducing gas concentration for gas i (in mol m^{-3}), n is the reaction order for each gas and k_{si} the kinetic constant for the reaction with gas i.

The reaction rate constant k_{si} takes the following Arrhenius form:

$$k_{si} = k_0 \exp\left(\frac{-E_a}{RT}\right) \tag{10}$$

where k_o is the pre-exponential factor, E_a represents the activation energy, R is the universal gas constant and T is the reacting temperature that is used in the experiment.

Fig. 5 shows the conversion curves obtained for the powdered materials (black lines) when modifying the molar concentration of each gas. Complete conversion is always quickly achieved with gas concentrations even with gas concentrations of 5 vol.% of reducing gas, and the graphs that represent the evolution of conversion shows almost straight slopes for all the concentrations tested. In addition, the material used as support has not an important effect on materials' reactivity and similar reduction conversion curves have been obtained for both materials.

The kinetic parameters n and k_{si} have been determined from the

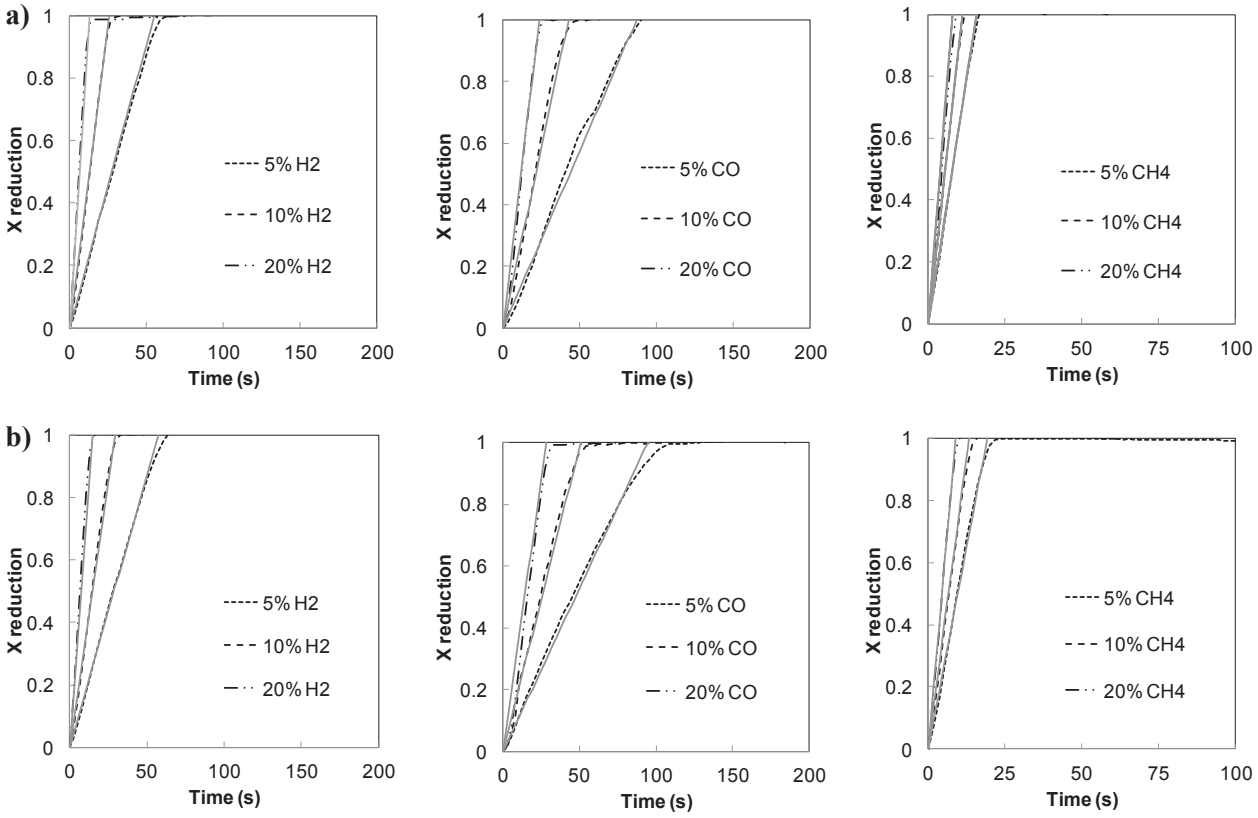

Fig. 5. Effect of gas concentration on reduction conversion curves of CuO-based powder materials with H_2, CO and CH_4 at 1123 K. a) Cu65Al_COP particles, b) Cu65MgAl_COP particles. *Discontinuous black lines are experimental results, continuous grey lines are SCM model predictions considering only chemical reaction control.*

Table 2
Kinetic parameters determined for the reduction reaction of the CuO-based materials supported onto Al_2O_3 and $MgAl_2O_4$.

	Cu65Al_COP particles and pellet			Cu65MgAl_COP particles and pellet		
	H_2	CO	CH_4	H_2	CO	CH_4
n	1 R2 = 0.9899	0.9 R2 = 0.9990	0.5 R2 = 0.9991	1 R2 = 0.9976	0.9 R2 = 0.9974	0.55 R2 = 0.9985
k_0, $mol^{1-n}\,cm^{3n-2}\,s^{-1}$	35 R2 = 0.9915	32 R2 = 0.9965	5 R2 = 0.9914	32 R2 = 0.9858	25 R2 = 0.9909	6R2 = 0.9919
EA, $kJ\,mol^{-1}$	10 ± 0.3	25 ± 0.4	60 ± 0.6	10 ± 0.3	26 ± 0.5	59.5 ± 0.5
b	1	1	4	1	1	4

experimental data shown in Figs. 4 and 5. In first place, the reaction order of each gas n has been determined from the slope of the representation of $\ln(\rho_b L/b\tau)$ versus $\ln(C_{gi})$ for the experiments shown in Fig. 5, which have been carried out at a constant temperature. The reaction orders regressed from these curves correspond to n = 1 for H_2, n = 0.9 for CO and n = 0.5 for CH_4. These values are in agreement with values reported by other authors for materials with lower Cu contents [28,32,39]. The parameters k_o and Ea for the kinetic constant k_{si} have been calculated by the experiments carried out on the effect of temperature in the reaction rates for a given reducing gas concentration. Considering the Arrhenius dependence previously mentioned, the representation of $\ln(k_0)$ vs 1/T allows calculating Ea from the slope and $\ln(k_0)$ by the intercept for each reacting gas. Results obtained for the kinetic parameters are summarized in Table 2. Practically the same kinetic parameters have been obtained for both Cu65Al_COP and Cu65MgAl_COP materials in powder form, as noticed in this table. As it was expected from the comparison of the curves shown in Fig. 4, higher activation energy values were obtained for the CH_4 (around 60 $kJ\,mol^{-1}$) with respect to the other gases (around 26 $kJ\,mol^{-1}$ for CO, 10 mol^{-1} for H_2) that showed a lower dependency with the reaction temperature. It has been found that although the activation energies as well as the reaction orders for the different reactions are in agreement with the results reported in literature, in the case of materials with significantly lower Cu content (10%wt of CuO) tested by other authors [32] the pre-exponential factors obtained for the reduction reactions with all the reducing agents tested presented lower values. Therefore the reaction rate (expressed as $mol^{1-n}\,cm^{3n-2}\,s^{-1}$) of the different reactions (with H_2, CO and CH_4, respectively) for the material with 10%wt of CuO content has been significantly lower than for the materials tested in this work with Cu contents around 82%wt of CuO. On the other hand, other authors [50] that have been analyzed the reduction kinetics of materials with different Cu contents, also have found a increase in the reaction rate with the increase of Cu load (between 25 and 75% of CuO) and lower values for the constant reaction rate than for the materials presented in this work has been also reported.

Grey curves included in Fig. 5 represents the SCM predictions when using the kinetic parameters determined. As noticed, good agreements between experimental curves and theoretical ones are obtained. Therefore it seems clear that the particles follow a SCM with kinetic regime for the three reducing gases tested.

Pellets made from the CuO-based particles have been also analyzed in this work as these materials are required for the operation of the fixed bed reactors in the Ca/Cu looping process. In order to elucidate the reaction pattern followed for the materials in the pellet form, cross section photographs of a single pellet were taken at different conversion levels on the course of the oxidation and reduction reactions (with H_2). Fig. 6 shows the photographs taken to the P_Cu65Al_COP material when being fully reduced (Fig. 6a), partially oxidized (Fig. 6b) and fully oxidized (Fig. 6c). As noticed, a clear external rim of oxidized material with a black colour and an inner core of reduced solid were clearly appreciated. In the same way, cross section photographs of a fully oxidized pellet that was partially reduced (Fig. 6d) and fully reduced (Fig. 6e) with H_2 were taken, which showed the same reaction pattern with a clear external rim of reduced material in reddish colour. Thereby, during the reduction reaction with H_2, a clear reaction front moves toward the inner part of the pellet where a core of unreacted material is present. In this way, a shrinking core model (SCM) pattern, that was also able to describe the oxidation reaction of these high loaded CuO-based materials [51], has been proposed to study the evolution of the different reduction reactions tested in this work. Both situations: a chemical reaction control or an intense diffusion control to the unreacted core of the pellet could produce the types of images shown in Fig. 6.

Based on the information from Fig. 6, a SCM with cylindrical geometry is proposed for explaining the reaction pattern of the materials in pellet form. Two possible scenarios have been considered: pure chemical reaction control and mixed control of internal diffusion and

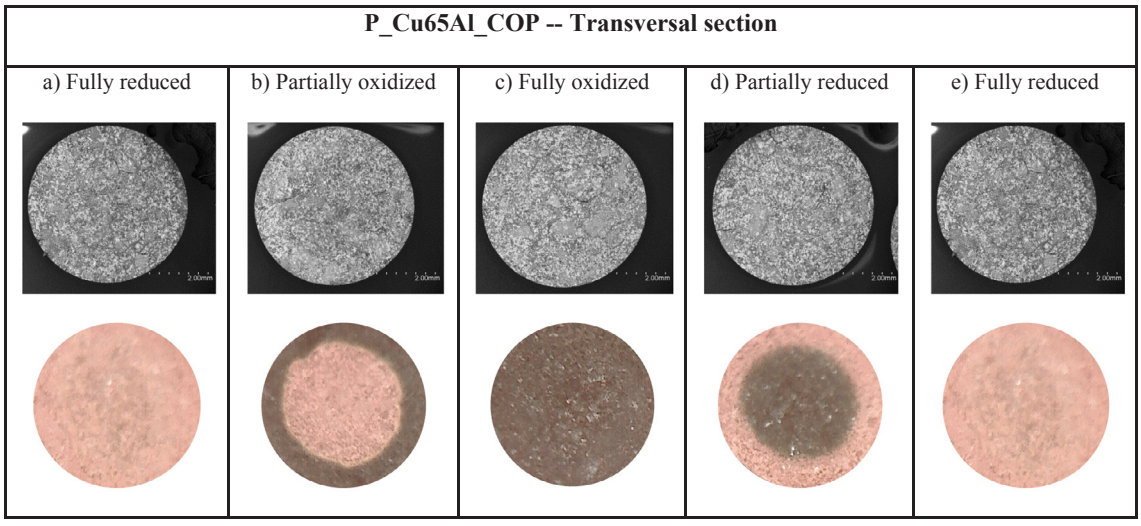

Fig. 6. SEM images and internal photographs of transversal section of the pellet P_Cu65Al_COP along the different steps of the reduction–oxidation process.

chemical reaction, in order to check which one predicts better the experimental curves obtained in TGA. Eq. (11) corresponds to a SCM with chemical reaction control and cylindrical geometry [49]. As anticipated before, the kinetic parameters obtained for powder materials (given in Table 2) have been incorporated in this expression 8 to evaluate the intrinsic character of these parameters.

$$\frac{t}{\tau_i} = 1-(1-X_{red})^{1/2} \tag{11}$$

On the other hand, a SCM with mixed control of internal diffusion and chemical reaction has been also applied. Taking into account the symmetry of the pellets, as well as the quite similar results obtained applying the cylindrical and spherical geometry for the pellets to the SCM with kinetic control (see Fig. 7), it has been considered a spherical geometry to explain the evolution of the reduction conversion of the pellets because of the simplicity of the global equation of the SCM considering mass transfer, internal diffusion and chemical reaction terms.

The model takes into account the following assumptions: (a) the particle is spherical and its volume is constant; (b) mass and density changes of the particle is expected to varied slightly as the reaction progresses; (c) the particle is isothermal; (d) the structure of the porous particle is uniform; (e) the porosity of the unreacted core is very small which means that the unreacted solid material is almost impervious to the reactant gases. Eq. (12) shows the general formula of the SCM model in terms of the change of the unreacted core radius (r_c) at any time taking into account the three main resistances [49] which may be involved in the reduction reactions.

$$\frac{dr_c}{dt} = -\frac{bC_{gi}}{\rho_b}\Big/\left[\frac{r_c^2}{L^2 h_m} + \frac{(L-r_c)r_c}{RD_e} + \frac{1}{k_{si}C_{gi}^{n-1}}\right] \tag{12}$$

where b is the stoichiometric coefficient of the CuO reduction reaction depending on the reacting gas evaluated, C_{gi} is the molar concentration of the gas species i (in mol m^{-3}), ρ_b is the molar density of the solid (in mol m^{-3}), L is the radius of the pellet, h_m represents the gas film mass transfer coefficient (in m s^{-1}), D_e represents the diffusivity of the gas species i through the layer of reacted material (in m^2/s), k_{si} is the reaction rate constant and n is the reaction order.

The three terms that appear in the denominator of the Eq. (12) are related with the mass-transfer, the internal (ash-layer) diffusion and the chemical reaction rate, respectively. Considering that no mass and density changes are produced in the pellet during reaction and that the experimental conditions have been selected to avoid external mass transfer the first term in denominator in the Eq. (9) can be neglected.

The effective diffusivity (D_e) that appears in the second term of the equation can be calculated from gas diffusivity and the structural properties of the porous material using the formula:

$$D_e = \varepsilon \cdot \frac{D_{pore}}{\tau_{pore}} \tag{13}$$

where D_{pore} represents the mass diffusivity inside the mesopore (in m^2/s), ε is the solid porosity and τ_{pore} is the tortuosity of the pores. The tortuosity of the materials have been determined using the correlation between porosity-tortuosity proposed by Matyka et al. [52]:

$$\tau_{pore} = \sqrt{\frac{2\varepsilon}{3[1-1.09(1-\varepsilon)^{2/3}} + \frac{1}{3}} \tag{14}$$

The gas diffusivity can be expressed as the combination of the bulk diffusivity (D_i) and the Knudsen diffusivity (D_{Kn}):

$$\frac{1}{D_{pore}} = \frac{1}{D_{Kn}} + \frac{1}{D_i} \tag{15}$$

The Knudsen diffusion has been determined by:

$$D_{Kn} = \frac{d_{pore}}{3} \cdot \sqrt{\frac{8R \cdot T}{\pi M_i}} \tag{16}$$

where d_{pore} and M_i are the pore diameter and the molecular weight of the gas i expressed in meters and kg/mol, respectively.

The bulk diffusivity is calculated by the FGS (Fuller, Schettler and Giddings) correlation [53] as follows:

$$D_i = \frac{0.01013 \cdot T^{1.75}\sqrt{M_i^{-1} + M_k^{-1}}}{P(\sqrt[3]{v_i} + \sqrt[3]{v_k})^2} \tag{17}$$

The values obtained for D_e and τ_{pore} for the different gases and for the two pelletized materials are shown in Table 3.

These values of D_e and τ_{pore}, and the kinetic parameters k_{si} and n determined for the materials in powder form when assuming a SCM with only chemical reaction control (shown in Table 2) have been included in Eq. (12) at each specific conditions of temperature and volume concentration of gas. In this way, the parameter r_c is the only unknown parameter in the Eq. (12) and the evolution of r_c as function of time is evaluated for each specific gas and conditions using the Runge-Kutta fourth-order method (RK4) programmed in Visual Basic. The theoretical results obtained by this model (continuous grey lines) are shown for the pellets in Fig. 9, respectively, together with the results predicted by the SCM that only considers chemical reaction control (continuous black lines) and the experimental values (discontinuous black lines).

Fig. 8 shows the effect of temperature from 973 K to 1143 K on the reduction conversion of the pellets with 10 vol.% of reducing gas in N_2. As expected, the conversion rate increased when increasing the reduction temperature. Complete conversion was reached in less than 250 s when using H_2 or CH_4 and this time increased until at least 500 s in the case of using CO, in agreement with the results of particles. Comparing the results obtained for both materials, faster reduction reaction rates with H_2 were observed for the Cu65MgAl_COP material than for the Al_2O_3-supported one. Complete reduction times of the order of 150 s were observed for the Cu65MgAl_COP, whereas for the Cu65Al_COP one this complete reduction times were larger, of the order of 220–250 s. This trend was completely reverted when using CH_4 as reducing gas, which resulted in faster reaction rates for the Cu65Al_COP material. On the overall, regardless of the gas used, the time for total conversion of pellets is about 10 times the time of conversion of particles, which can be noticed if comparing results in Figs. 4 and 8.

Fig. 9 shows the conversion results obtained when modifying the reducing gas concentration at 1123 K (discontinuous black lines) for the two materials in pellet form. In this figure it has been included also the model predictions of the SCM considering pure chemical reaction

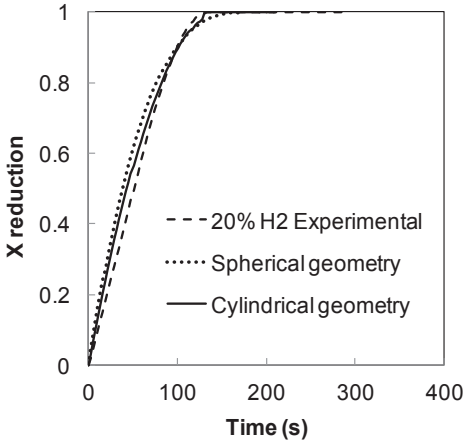

Fig. 7. Comparison between the results obtained considering spherical and cylindrical geometry for the symmetrical pellets P_Cu65Al_COP with 20%vol. H_2 (1 bar, 1123 K).

Table 3
Effective diffusivity and tortuosity values determined for the two pellets tested.

	P_Cu65Al_COP	P_Cu65MgAl_COP
De (m^2/s) for H_2	4.95×10^{-5}	2.02×10^{-4}
De (m^2/s) for CO	1.32×10^{-5}	5.39×10^{-5}
De (m^2/s) for CH_4	1.74×10^{-5}	7.05×10^{-5}
τ_{pore}	1.14	1.10

control (continuous black lines) given in Eq. (11) and considering mixed chemical reaction and diffusion control (continuous grey lines) indicated in Eq. (12). Particularly for the CuO-based material supported on $MgAl_2O_4$, a second marked slope could be observed when using CO and CH_4 as reducing gases. This variation of the slope during reduction reaction with CH_4 and CO is more pronounced at low reacting gas concentrations which indicates that gas diffusion resistance to the unreacted core of the particle becomes more important at concentrations below 10%vol. of CH_4 and CO. In fact, as appreciated from the SCM predictions shown in this Figure, the SCM model considering mixed chemical reaction and gas diffusion control (i.e. model given in Eq. (12)) predicts pretty well the reduction conversion curves obtained for the Cu65MgAl_COP when using CO and CH_4 as reducing gases. However, if looking to the reduction conversion curves with H_2 for this CuO-material, the SCM with pure chemical reaction control fits reasonably well the experimental conversion curves for this material. Finally, comparing the conversion curves obtained for the two materials, it is noticed that the inert support has an effect on the pellet's reactivity, being the complete reaction times lower for the Al_2O_3-supported material than for the $MgAl_2O_4$-supported one. For the case of the Cu65Al_COP pellets, the SCM with pure chemical reaction control fits better the experimental curves than the combined chemical reaction and gas diffusion control SCM model for any of the reducing gas used.

3.2. Reduction tests with process gas composition

Once the reduction kinetics for the materials evaluated have been determined, they were validated with two additional tests using a mixture of H_2, CO and CH_4 during the reduction as in the real process conditions of the calcination/reduction stage of the Ca/Cu process. The idea behind these reduction tests was investigating the effect of reducing gases mixtures (H_2, CO and/or CH_4) in the conversion curves. A first test with typical gas composition from an intermediate cooling stage between reduction/calcination and SER steps of the Ca/Cu process (70.4%vol. H_2, 26.4%vol. CO and 1.3%vol. CH_4 at 1143 K and 1 bar), and a second test with the typical gas composition exiting from an adiabatic pre-reforming stage (45%vol. CH_4, 7.3%vol. H_2, 10%vol. CO_2 and 37.7%vol. N_2 at 1143 K and 1 bar) have been carried out. Fig. 10 represents the comparison between the experimental results obtained for the Cu65Al_COP material using such syngas composition as reducing gas (symbols) and the SCM model prediction curves (black lines).

In this case, the time needed to reach complete conversion for each individual gas (i.e. τ_i) was determined using Eq. (9) with the corresponding kinetic parameters for such gas given in Table 2. Then, the complete reaction time for the pellet in the gas mixture is assumed to be calculated as in Eq. (18), as the sum of the reactivities of each gas individually.

$$\tau_{mix} = \frac{1}{\frac{1}{\tau_{H2}} + \frac{1}{\tau_{CO}} + \frac{1}{\tau_{CH4}}} \tag{18}$$

This expression considers that the reduction with the three gases takes place simultaneously, taking into account the trend observed by other authors [54]. The prediction of the curves shown in Fig. 10 corroborates that the evolution of conversion of the pellet can be suitably predicted by the sum of the contribution of each gas in the reaction.

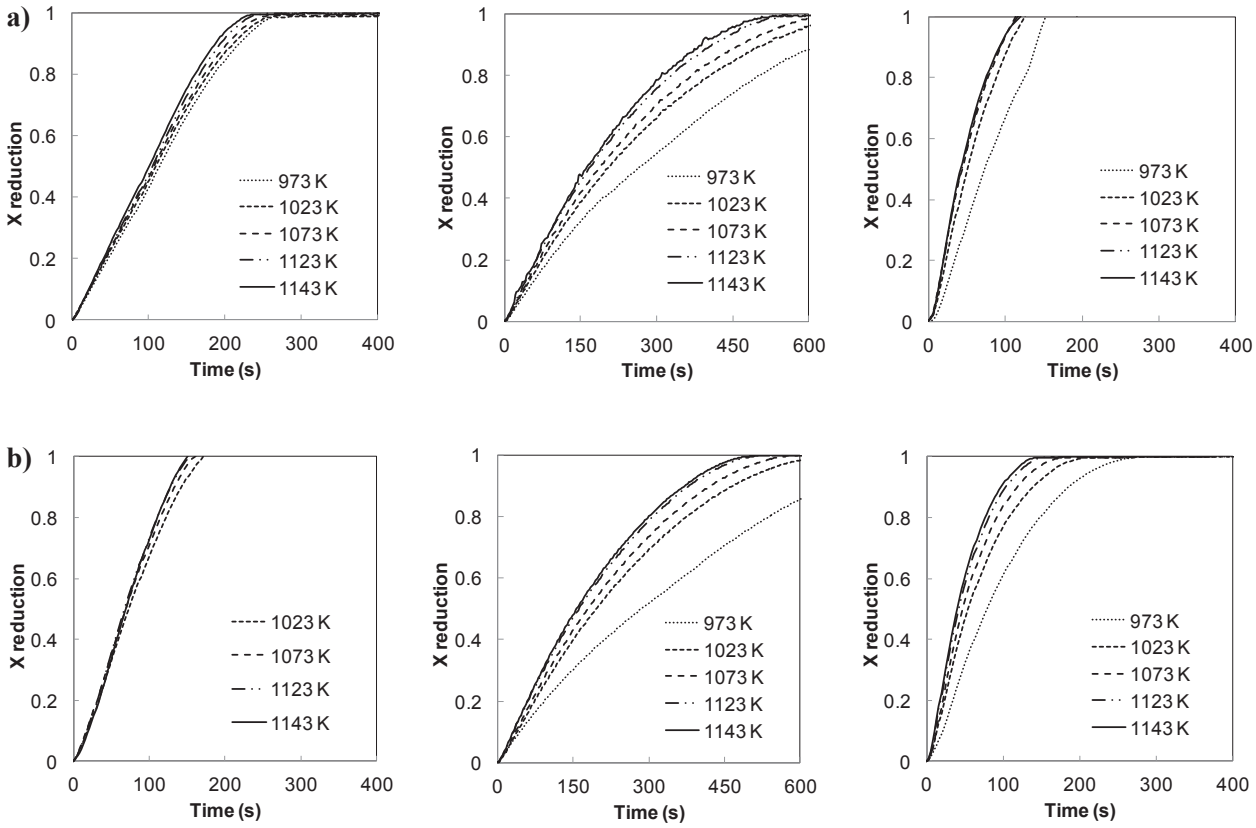

Fig. 8. Effect of temperature on reduction conversion curves of CuO-based pellets. a) P_Cu65Al_COP, b) P_Cu65MgAl_COP : (left) 10% vol. H_2; (center) 10% vol. CO; (right) 10% vol. CH_4 in N_2.

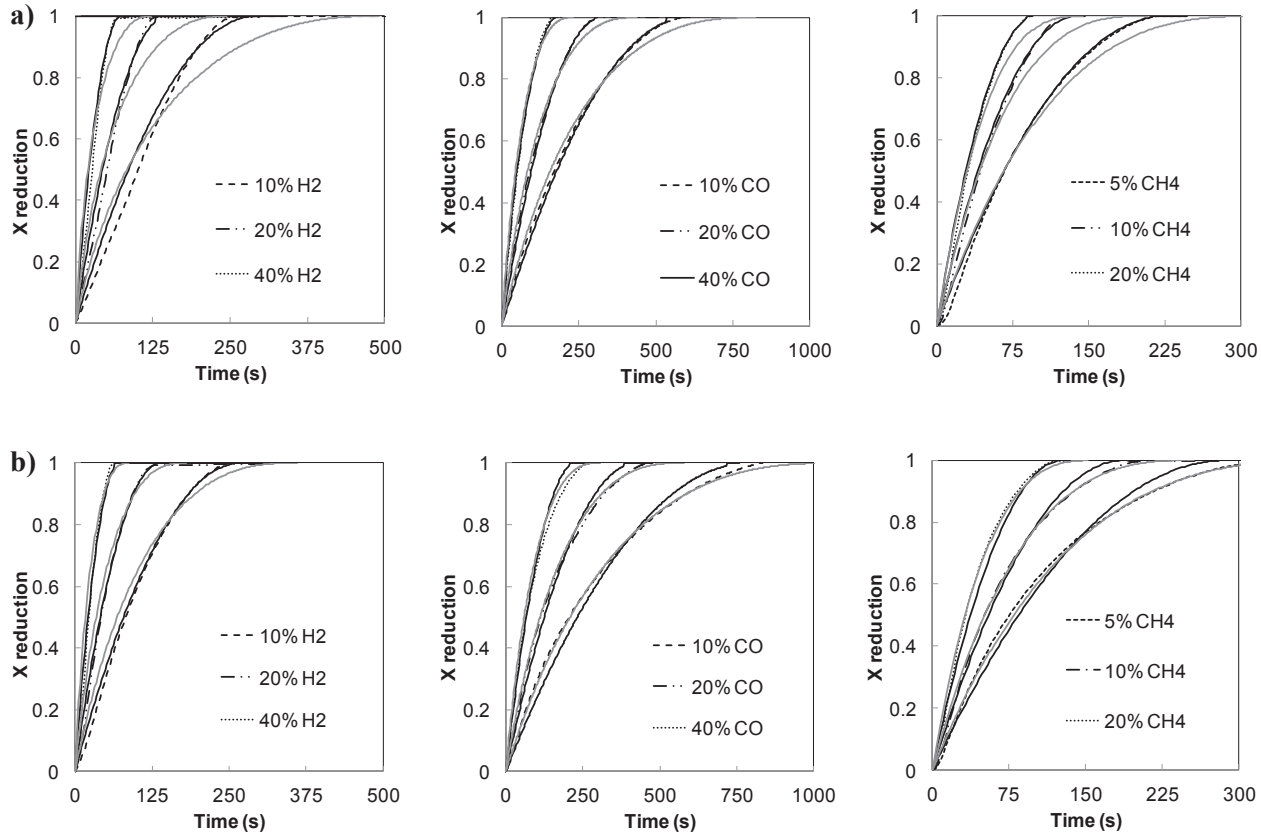

Fig. 9. Effect of gas concentration on reduction conversion curves of CuO-based pellets with H_2, CO and CH_4 at reaction temperature of 1123 K. a) P_Cu65Al_COP, b) P_Cu65MgAl_COP. Discontinuous black lines are experimental results, continuous black lines are SCM predictions considering pure chemical reaction control and continuous grey lines are SCM predictions considering mixed control of chemical reaction and diffusion.

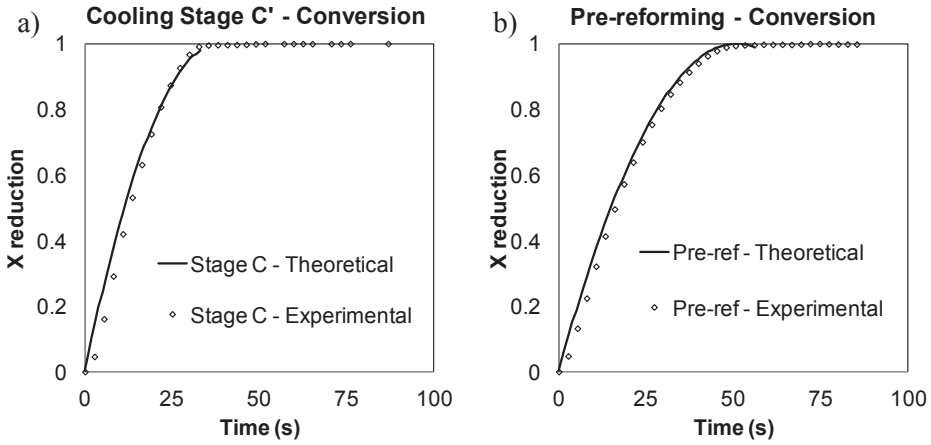

Fig. 10. Evaluation of the experimental and theoretical conversion of the P_Cu65Al_COP for two different syngas compositions coming from a: (a) cooling stage C′, and (b) adiabatic pre-reforming.

The reduction conversion curves for the pellets of the $MgAl_2O_4$ supported material (i.e. Cu65MgAl_COP) have been also calculated following the same procedure to calculate τ_{mix} as that explained to Cu65Al_COP material. Fig. 11 shows the comparison between the conversion curves for both pellets for the syngas composition coming from a subsequent cooling/reforming stage (referred as stage C' in most of the Ca/Cu related works) and from an adiabatic pre-reforming. As it can be observed, faster reduction kinetics resulted for the Al_2O_3-supported material (continuous lines) than for the $MgAl_2O_4$ one (discontinuous lines), as already seen experimentally in Fig. 9. However, in any of the cases, conversion of the pellets is extremely fast and complete conversion can be achieved in less than 100 s.

Finally, a simplified analysis about the coupling between the heat released by the reduction of the CuO-based material and the heat demand by the $CaCO_3$ calcination within a reduction/calcination stage of the Ca/Cu process has been carried out. This analysis has been performed assuming that the CuO reduction and the $CaCO_3$ calcination take place at the same temperature to analyze how the heat involved in each reaction could influence the evolution of the reaction front along the reactor.

In this way, the reduction reaction enthalpies for the CuO reduction with a mixture of H_2, CH_4 and CO (Eqs. (3)–(5)) have been calculated.

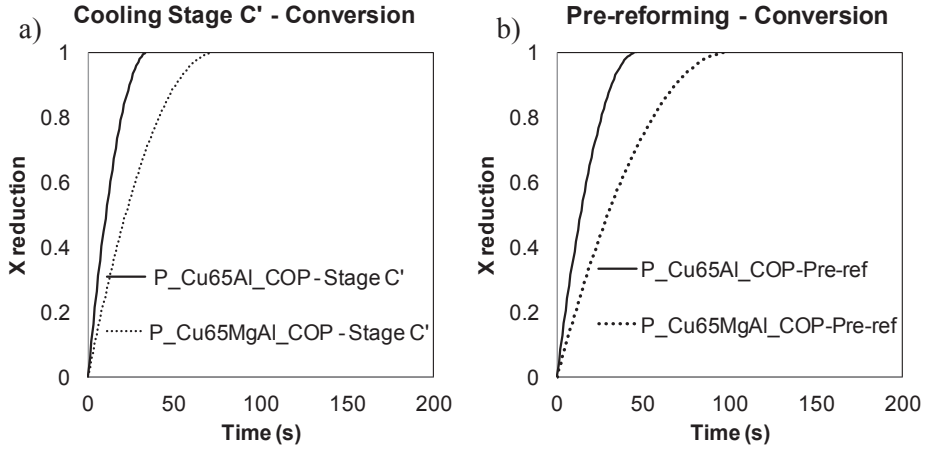

Fig. 11. Comparison of the conversion curves predicted by the SCM for the P_Cu65Al_COP and P_Cu65MgAl_COP for two different syngas compositions coming from a: (a) cooling stage C′, and (b) adiabatic pre-reforming.

The value of the global enthalpy of the reduction reaction within the reduction/calcination step has been determined as −108.19 kJ/mol CuO at 1143 K and 1 bar, taking into account the gas composition coming from a subsequent cooling/reforming step (i.e. 70.4 vol.% H_2, 26.4 vol.% CO and 1.3 vol.% CH_4) [24]. This value is fairly constant for the range of temperatures of interest (−109.17 kJ/mol CuO at 1188 K). The heat released by the pellet during the course of the reduction reactions has been determined taking into account the moles of oxygen released during each reaction and the global reaction enthalpy at the specific temperature and gas composition conditions for every step. The total heat released by one Cu-based pellet during the reduction reactions that take place during this reduction/calcination step has been experimentally determined as 67.4 J that are released in a period of approximately 40 s for the range of temperatures of interest for this process stage (1123 K–1188 K). The heat release rate (J/s) with time for an oxidized pellet will not present noticeable variations for this temperature range, given the fact that the activation energies for reactions in Eqs. (3)–(5) are low (see Table 2 for kinetic parameters). Therefore, for the sake of simplicity, only the heat release rate (J/s) with time of an oxidized P_Cu65Al_COP pellet at 1143 K has been plotted in Fig. 12a) and b).

The Fig. 12a) also includes the energy needed for the calcination of $CaCO_3$ at three different temperatures. A typical Cu/Ca molar ratio of 2, that would be suitable for the reducing gas composition tested, has been assumed to calculate the energy demand (J/s) of the calcination reaction with time. The intrinsic calcination kinetics have been taken from the literature [48], neglecting for this figure the presence of gas diffusion of the CO_2 produced through the porous structure of the CaO-material pellet. In this way, the kinetic parameters obtained in this work for a limestone with 96.1%wt of CaO, 1.2%wt of MgO and 1.1%wt of SiO_2 (named as limestone A in [48] has been used to analyze the evolution of calcination conversion. Therefore the evolution of calcination reaction was evaluated considering a pre-exponential factor of 2056970.3 m^3/kmol s and a activation energy of 112 kJ/mol for the limestone. These parameters were included in the Arrhenius correlation (10) to determine the reaction rate constant (k_{calc}) and then the calcination conversion was predicted using the following formula [48]:

$$Xcalc = 1-(1-\left(\frac{1}{3}\cdot k_{calc}\cdot t\cdot(C_{CO2,g}-C_{CO2,eq}\right)^3 \quad (19)$$

where t is represents the time, $C_{CO2,g}$ is the partial pressure of CO_2 in the gas and $C_{CO2,eq}$ represents the partial pressure of CO_2 in the equilibrium.

For calculating the heat demand curve for the calcination reaction a CO_2 partial pressure of 0.4 bar is considered and a value of 178 kJ/mol for the calcination reaction, which corresponds to the typical conditions expected at this reduction/calcination stage outlet [24]. The activation energy for the calcination reaction is high (112 kJ/mol $CaCO_3$) when compared with the activation energies for the reduction reactions. This means that the energy demanded (in J/s) by the calcination has a strong dependence with temperature.

Several operating temperatures have considered for the calcination predictions (see Fig. 12a) and b)). In addition, the possibility of find a slightly lower calcination reaction during the operation of the Ca-Cu

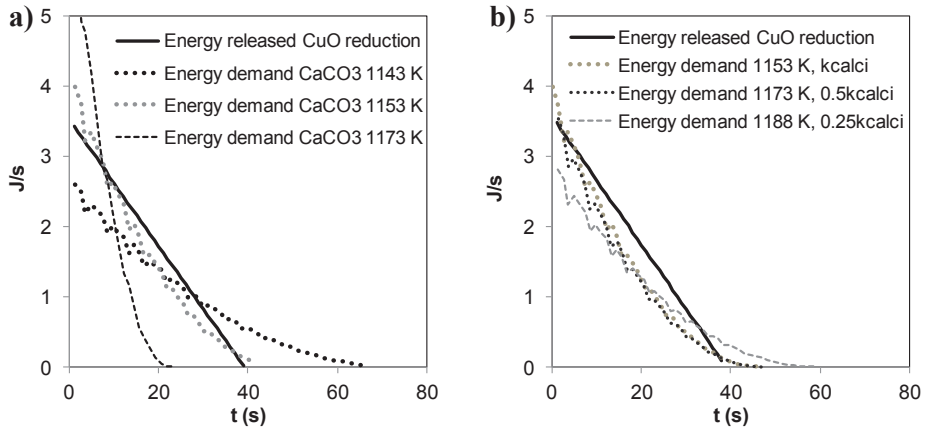

Fig. 12. a) Comparison between energy released and energy demand for the pellet P_Cu65Al_COP under conditions of the step C; b) Sensitivity analysis of the predictions with the calcination kinetic constant at different temperatures under conditions of the step C.

process has been taken into account considering also lower values than the theoretical for the calcination rate constant.

According to the Fig. 12a), the best match between the energy release rate and the energy demand one takes place at 1153 K. The data in Fig. 12a) also show that when a larger temperature of 1173 K is considered for the calcination reaction, which may represent a situation where the reduction reaction has proceeded faster causing a temperature increase in the solid bed, the calcination reaction is accelerated. However, such temperature increase is not enough for balancing the thermal balance in the solid bed and the reaction fronts of both reduction and calcination reaction would not evolve together along the bed. On the other hand, if the calcination reaction is considered at 1143 K, there is a heat excess during the initial seconds that would increase the temperature and accelerate the calcination rate, being again both reaction fronts only close at 1153 K.

Fig. 12b) shows a sensitivity analysis with respect to the calcination kinetic constant. As mentioned before, the intrinsic kinetics for the calcination reaction were taken for calculating the heat demand rate of this reaction in Fig. 12a). However, due to the fact that the functional materials used for this process will be used in pellet form, diffusion of the CO_2 released from this reaction towards the bulk phase may slow down the kinetics of this reaction. To account for this effect, the possibility of having a reduced calcination kinetic constant has been analyzed in this figure. As appreciated, a higher bed temperature would be required to synchronize both reaction fronts when slower kinetics for the calcination reaction are considered. On view of the experimental results obtained, the Cu based material presented in this work has shown adequate reduction kinetics to sustain a reduction/calcination stage under suitable operation conditions for the Ca/Cu process [55].

4. Conclusions

In this work, the reduction of CuO with H_2, CO and CH_4 under the conditions of interest for the reduction/calcination stage of the Ca/Cu looping process has been investigated in a TGA for two different CuO-based materials using different support with a high Cu content (i.e. around 65%wt of Cu) both in particle and pellet form. The kinetic parameters for the reduction reactions have been determined for the materials in powder using a SCM with chemical reaction control. It was found that the reduction reaction of the powdered materials with CH_4 showed a greater variation with temperature, and therefore the highest values of activation energy were obtained for the reduction reaction of the materials with this gas.

For the materials in pellet form, it was assessed whether the effect of internal gas diffusion influences the kinetics or not. It was demonstrated that for the Al_2O_3-supported material, the reduction reaction was kinetically controlled for the temperature range studied (973–1143 K) regardless of the reducing gas used. On the contrary, for the $MgAl_2O_4$-based material, the internal diffusion resistance becomes important for the reduction reactions with CO and CH_4 and so a combined chemical reaction/gas diffusion control regime needs to be considered. Therefore, it seems that the reducing gas has a worst access to the copper active sites in the case of the pellets supported on to $MgAl_2O_4$. This effect could be related with a greater decrease in the CuO and $MgAl_2O_4$ crystal size after cycles which has not been so pronounced in the case of the CuO and $CuAl_2O_4$ crystals of the material onto Al_2O_3; and also with the lower porosity of the material supported over $MgAl_2O_4$.

The evolution of the reduction conversion of the pellet supported on Al_2O_3 when using a syngas composition from a subsequent cooling/reforming step and from an adiabatic pre-reforming has been successfully fitted using the kinetic parameters previously calculated. Finally, the coupling between the energy released during the reduction of one pellet of the CuO-based material and the energy demand from the calcination has been analyzed. Results obtained indicate that the calcination and reduction reaction fronts could closely advance throughout the solid bed under proper conditions of temperature, which would avoid large peaks of released heat within the bed that may cause problems if the temperature reached exceeds certain limits.

Acknowledgments

This work acknowledges the support by European Union Seventh Frame Programme FP7 under grant agreement n° 608512 (ASCENT Project). Laura Díez-Martín acknowledges the FPI fellowship (ENE 2012-37936-CO2-01, BES-2013-064616 financed by MINECO).

References

[1] IEA. Technology Roadmap. Hydrogen and Fuel Cells. IEA Publications, France. Available from: https://www.iea.org/publications/freepublications/publication/TechnologyRoadmapHydrogenandFuelCells.pdf; 2015.
[2] Meerman JC, Hamborg ES, van Keulen T, Ramírez A, Turkenburg WC, Faaij APC. Techno-economic assessment of CO2 capture at steam methane reforming facilities using commercially available technology. Int J Greenhouse Gas Control 2012;9(Suppl C):160–71.
[3] Romano MC, Anantharaman R, Arasto A, Ozcan DC, Ahn H, Dijkstra JW, et al. Application of advanced technologies for CO2 capture from industrial sources. Energy Procedia 2013;37(Suppl C):7176–85.
[4] Weydahl T, Jamaluddin J, Seljeskog M, Anantharaman R. Pursuing the pre-combustion CCS route in oil refineries – the impact on fired heaters. Appl Energy 2013;102(Suppl C):833–9.
[5] IPCC. Fifth Assessment Report of the Intergovernmental Panel on Climate Change. Available from: http://www.ipcc.ch/report/ar5/wg3/; 2014.
[6] Rostrup-Nielsen JR, Rostrup-Nielsen T. Large-scale hydrogen production. CATTECH 2002;6(4):150–9.
[7] Abanades JC, Murillo R, Fernandez JR, Grasa G, Martínez I. New CO2 capture process for hydrogen production combining Ca and Cu chemical loops. Environ Sci Technol 2010;44(17):6901–4.
[8] Chen Z, Grace JR, Lim CJ. CO2 capture and hydrogen production in an integrated fluidized bed reformer-regenerator system. Ind Eng Chem Res 2011;50(8):4716–21.
[9] Fernández JR, Abanades JC, Murillo R, Grasa G. Conceptual design of a hydrogen production process from natural gas with CO2 capture using a Ca–Cu chemical loop. Int J Greenhouse Gas Control 2012;6:126–41.
[10] Martínez I, Romano MC, Chiesa P, Grasa G, Murillo R. Hydrogen production through sorption enhanced steam reforming of natural gas: thermodynamic plant assessment. Int J Hydrogen Energy 2013;38(35):15180–99.
[11] Weimer T, Berger R, Hawthorne C, Abanades JC. Lime enhanced gasification of solid fuels: examination of a process for simultaneous hydrogen production and CO2 capture. Fuel 2008;87(8):1678–86.
[12] Han C, Harrison DP. Simultaneous shift reaction and carbon dioxide separation for the direct production of hydrogen. Chem Eng Sci 1994;49(24, Part 2):5875–83.
[13] Hufton JR, Mayorga S, Sircar S. Sorption-enhanced reaction process for hydrogen production. AIChE J 1999;45(2):248–56.
[14] Yi KB, Harrison PD. Low-Pressure Sorption-Enhanced Hydrogen Production. 2005.
[15] Balasubramanian B, Lopez A, kaytakoğlu S, Harrison PD. Hydrogen from methane in a single-step process. 1999.
[16] Abanades JC, Murillo VR. Method for recovering co2 by means of Cao and the exothermic reduction of a solid. 2009.
[17] Fernandez JR, Abanades JC, Grasa G. Modeling of sorption enhanced steam methane reforming—Part II: simulation within a novel Ca/Cu chemical loop process for hydrogen production. Chem Eng Sci 2012;84:12–20.
[18] Fernández JR, Abanades JC, Murillo R. Modeling of Cu oxidation in adiabatic fixed-bed reactor with N2 recycling in a Ca/Cu chemical loop. Chem Eng J 2013;232:442–52.
[19] Alarcón JM, Fernández JR. CaCO3 calcination by the simultaneous reduction of CuO in a Ca/Cu chemical looping process. Chem Eng Sci 2015;137:254–67.
[20] Fernández JR, Abanades JC. Overview of the Ca–Cu looping process for hydrogen production and/or power generation. Curr Opin Chem Eng 2017;17(Suppl C):1–8.
[21] Alarcón JM, Fernández JR, Abanades JC. Study of a Cu-CuO chemical loop for the calcination of CaCO3 in a fixed bed reactor. Chem Eng J 2017;325(Suppl C):208–20.
[22] Martínez I, Romano MC, Fernández JR, Chiesa P, Murillo R, Abanades JC. Process design of a hydrogen production plant from natural gas with CO2 capture based on a novel Ca/Cu chemical loop. Appl Energy 2014;114:192–208.
[23] Martínez I, Murillo R, Grasa G, Fernández JR, Abanades JC. Integrated combined cycle from natural gas with CO2 capture using a Ca–Cu chemical loop. AIChE J 2013;59(8):2780–94.
[24] Fernández JR, Abanades JC. Optimized design and operation strategy of a CaCu chemical looping process for hydrogen production. Chem Eng Sci 2017;166:144–60.
[25] Martini M, van den Berg A, Gallucci F, van Sint Annaland M. Investigation of the process operability windows for Ca-Cu looping for hydrogen production with CO2 capture. Chem Eng J 2016;303(Suppl C):73–88.
[26] Martini M, Martínez I, Romano MC, Chiesa P, Gallucci F, van Sint Annaland M. Increasing the carbon capture efficiency of the Ca/Cu looping process for power production with advanced process schemes. Chem Eng J 2017;328:304–19.
[27] Adánez J, de Diego LF, García-Labiano F, Gayán P, Abad A, Palacios JM. Selection

of oxygen carriers for chemical-looping combustion. Energy Fuels 2004;18(2):371–7.
[28] García-Lario AL, Martínez I, Murillo R, Grasa G, Fernández JR, Abanades JC. Reduction kinetics of a high load Cu-based pellet suitable for Ca/Cu chemical loops. Ind Eng Chem Res 2013;52(4):1481–90.
[29] Imtiaz Q, Kierzkowska AM, Broda M, Müller CR. Synthesis of Cu-rich, Al2O3-stabilized oxygen carriers using a coprecipitation technique: redox and carbon formation characteristics. Environ Sci Technol 2012;46(6):3561–6.
[30] Bhattacharyya R, Bhanja K, Mohan S. Mathematical analysis of reduction of copper oxide pellets by hydrogen using the shrinking core model. Fusion Eng Des 2015;100:560–4.
[31] García-Labiano F, Adánez J, de Diego LF, Gayán P, Abad A. Effect of pressure on the behavior of copper-, iron-, and nickel-based oxygen carriers for chemical-looping combustion. Energy Fuels 2006;20(1):26–33.
[32] García-Labiano F, de Diego LF, Adánez J, Abad A, Gayán P. Reduction and oxidation kinetics of a copper-based oxygen carrier prepared by impregnation for chemical-looping combustion. Ind Eng Chem Res 2004;43(26):8168–77.
[33] Go KS, Son SR, Kim SD. Reaction kinetics of reduction and oxidation of metal oxides for hydrogen production. Int J Hydrogen Energy 2008;33(21):5986–95.
[34] Goldstein EA, Mitchell RE. Chemical kinetics of copper oxide reduction with carbon monoxide. Proc Combust Inst 2011;33(2):2803–10.
[35] Hamers HP, Gallucci F, Williams G, Cobden PD, van Sint Annaland M. Reactivity of oxygen carriers for chemical-looping combustion in packed bed reactors under pressurized conditions. Energy Fuels 2015;29(4):2656–63.
[36] Ishida M, Wen CY. Comparison of kinetic and diffusional models for solid-gas reactions. AIChE J 1968;14(2):311–7.
[37] Liu X, Song F, Wen Z. A novel dimensionless form of unreacted shrinking core model for solid conversion during chemical looping combustion. Fuel 2014;129:231–7.
[38] Mattisson T. Materials for chemical-looping with oxygen uncoupling. ISRN Chem Eng 2013;2013:19.
[39] Maya JC, Chejne F. Modeling of oxidation and reduction of a copper-based oxygen carrier. Energy Fuels 2014;28(8):5434–44.
[40] Noorman S, Gallucci F, van Sint Annaland M, Kuipers JAM. A theoretical investigation of CLC in packed beds. Part 1: particle model. Chem Eng J 2011;167(1):297–307.
[41] Ortiz M, Gallucci F, Melchiori T, Spallina V, Annaland M. Kinetics of the Reactions Prevailing during Packed-Bed Chemical Looping Combustion of Syngas using Ilmenite. 2016.
[42] Qin C, Yin J, Liu W, An H, Feng B. Behavior of CaO/CuO based composite in a combined calcium and copper chemical looping process. Ind Eng Chem Res 2012;51(38):12274–81.
[43] San Pio MA, Gallucci F, Roghair I, van Sint Annaland M. Gas-solids kinetics of CuO/Al2O3 as an oxygen carrier for high-pressure chemical looping processes: the influence of the total pressure. Int J Hydrogen Energy 2017;42(17):12111–21.
[44] San Pio MA, Gallucci F, Roghair I, van Sint Annaland M. On the mechanism controlling the redox kinetics of Cu-based oxygen carriers. Chem Eng Res Des 2017;124:193–201.
[45] Qin C, Feng B, Yin J, Ran J, Zhang L, Manovic V. Matching of kinetics of CaCO3 decomposition and CuO reduction with CH4 in Ca–Cu chemical looping. Chem Eng J 2015;262:665–75.
[46] Díez-Martín L, Grasa G, Murillo R, Scullard A, Williams G. Development of suitable CuO-based materials supported on Al2O3, MgAl2O4, and ZrO2 for Ca/Cu H2 production process. Ind Eng Chem Res 2018.
[47] Patterson AL. The Scherrer formula for X-ray particle size determination. Phys Rev 1939;56(10):978–82.
[48] Martínez I, Grasa G, Murillo R, Arias B, Abanades J. Kinetics of Calcination of Partially Carbonated Particles in a Ca-Looping System for CO2 Capture. 2012.
[49] Levenspiel O. Chemical reactor engineering. Third ed. Wiley; 1998.
[50] Moghtaderi B, Song H. Reduction properties of physically mixed metallic oxide oxygen carriers in chemical looping combustion. Energy Fuels 2010;24(10):5359–68.
[51] Díez-Martín L, Grasa G, Murillo R, Martini M, Gallucci F, Annaland M. Determination of the oxidation kinetics of high loaded CuO-based materials under suitable conditions for the Ca/Cu H2 production process. 2018.
[52] Matyka M, Koza Z. How to Calculate Tortuosity Easily? 2012.
[53] Fuller EN, Schettler PD, Giddings JC. New method for prediction of binary gas-phase diffusion coefficients. Ind Eng Chem 1966;58(5):18–27.
[54] Abad Secades A, Adánez Elorza J, Diego Poza LFd, García Labiano F, Gayán Sanz P. Reduction kinetics of Cu-, Ni-, and Fe-based oxygen carriers using syngas (CO + H2) for chemical-looping combustion. 2007.
[55] Fernández JR, Abanades JC. Optimized design and operation strategy of a Ca-Cu chemical looping process for hydrogen production. Chem Eng Sci 2017;166:144–60.